JACS
JOURNAL OF THE AMERICAN CHEMICAL SOCIETY
Article
pubs.acs.org/JACS

High Proton Conduction at above 100 °C Mediated by Hydrogen Bonding in a Lanthanide Metal–Organic Framework

Qun Tang,[†] Yiwei Liu,[†] Shuxia Liu,*[,†] Danfeng He,[†] Jun Miao,[†] Xingquan Wang,[†] Guocheng Yang,[‡] Zhan Shi,[§] and Zhiping Zheng*[,∥,⊥]

[†]Key Laboratory of Polyoxometalate Science of the Ministry of Education, College of Chemistry, Northeast Normal University, Changchun, Jilin 130024, China

[‡]School of Chemistry and Life Science, Changchun University of Technology, Changchun, Jilin 130012, China

[§]State Key Laboratory of Inorganic Synthesis and Preparative Chemistry, College of Chemistry, Jilin University, Changchun, Jilin 130012, China

[∥]Frontier Institute of Science and Technology, Xi'an Jiaotong University, Xi'an, Shaanxi 710054, China

[⊥]Department of Chemistry and Biochemistry, University of Arizona, Tucson, Arizona 85721, United States

Supporting Information

ABSTRACT: A lanthanide metal–organic framework (MOF) compound of the formulation $[Eu_2(CO_3)(ox)_2(H_2O)_2]\cdot 4H_2O$ (**1**, ox = oxalate) was prepared by hydrothermal synthesis with its structure determined crystallographically. Temperature-dependent but humidity-independent high proton conduction was observed with a maximum of 2.08×10^{-3} S cm^{-1} achieved at 150 °C, well above the normal boiling point of water. Results from detailed structural analyses, comparative measurements of conductivities using regular and deuterated samples, anisotropic conductivity measurements using a single-crystal sample, and variable-temperature photoluminescence studies collectively establish that the protons furnished by the Eu(III)-bound and activated aqua ligands are the charge carriers and that the transport of proton is mediated along the crystallographic *a*-axis by ordered hydrogen-bonded arrays involving both aqua ligands and adjacent oxalate groups in the channels of the open framework. Proton conduction was enhanced with the increase of temperature from room temperature to about 150 °C, which can be rationalized in terms of thermal activation of the aqua ligands and the facilitated transport between aqua and adjacent oxalate ligands. A complete thermal loss of the aqua ligands occurred at about 160 °C, resulting in the disintegration of the hydrogen-bonded pathway for proton transport and a precipitous drop in conductivity. However, the structural integrity of the MOF was maintained up to 350 °C, and upon rehydration, the original structure with the hydrogen-bonded arrays was restored, and so was its high proton-conduction ability.

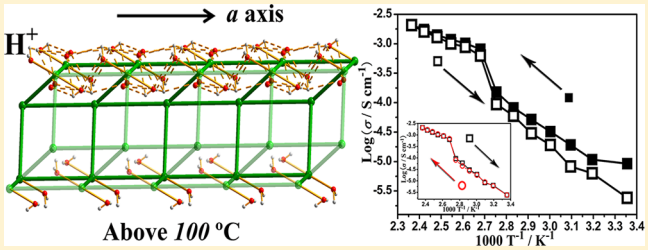

INTRODUCTION

The appealing application of fuel cells for clean energy production has stimulated the continuous exploration of new proton-transporting material.[1−4] In this context, the recent burgeoning research on proton-conducting metal–organic frameworks (MOFs) is notable, not merely because such efforts represent a distinct departure from the extensive work on their gas adsorption and separation,[5] catalysis,[6] and sensing properties,[7] but also because there exists the real potential of discovering new conducting materials for fuel cell applications.[8−10]

Of the proton-conducting MOFs reported, most are filled with proper proton-transfer media (e.g., NH_4^+, H_2O and H_3O^+) in well-defined channels and operate at room temperature and under high-humidity conditions (close to 100% relative humidity (RH)),[11−15] while the rest, being anhydrous, work independent of humidity at high temperatures (100–250 °C).[16,17] We note that the performance of water-mediated proton-conducting MOFs depends critically on the working temperature, as their conductivity drops substantially at temperatures above 100 °C due to the loss of water. To the best of our knowledge, hydrated MOFs capable of functioning at above 100 °C are not yet known, and the study of water-mediated proton transport in MOFs at temperatures well above the normal boiling point of water is not only fundamentally intriguing, but also practically significant as intermediate-temperature proton-conducting materials have been sought for new fuel cell designs.

In this work, we report for the first time such a unique example, $[Eu_2(CO_3)(ox)_2(H_2O)_2]\cdot 4H_2O$ (**1**, ox = oxalate), a lanthanide-containing MOF that exhibits humidity-independent proton conduction that increased with the enhancement of working temperatures. The highest proton conductivity was achieved at about 150 °C, well above the normal boiling point of water. Mechanistic studies establish that proton be the

Received: July 10, 2014
Published: August 19, 2014

   dx.doi.org/10.1021/ja5069855 | J. Am. Chem. Soc. 2014, 136, 12444–12449

charge carrier and ordered one-dimensional (1D) hydrogen-bonding arrays within the channels of the framework structure mediate the observed high proton conduction.

RESULTS AND DISCUSSION

Structural Analysis. Compound **1** of the crystallographic formula $[Eu_2(CO_3)(ox)_2(H_2O)_2]\cdot 4H_2O$ with its composition supported by elemental analyses (C, H and Eu) was prepared by a hydrothermal route in good yield. Crystallizing in space group $P\bar{1}$, its asymmetric unit comprises two independent Eu(III) ion centers, one carbonato, two oxalate, and two aqua ligands, in addition to four water molecules of crystallization. As shown in Figure 1, atom Eu(1) is nonacoordinate, featuring

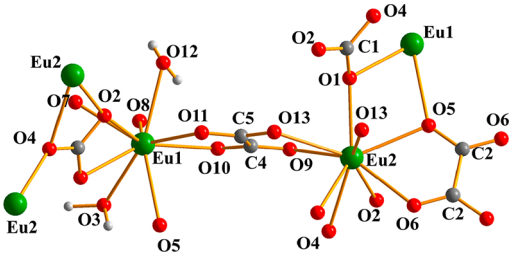

Figure 1. Representation of the Eu^{3+} coordination environments in the crystal structure of compound **1**.

coordination by five oxalate, two carbonato, and two aqua O atoms (O3 and O12); the Eu1−O distances range from 2.430(5) to 2.654(4) Å with the two involving the aqua ligands (Eu1−O3 = 2.546(3) Å and Eu1−O12 = 2.550(3) Å) being noticeably longer than those with the oxalate ligands and barring Eu1−O5 (2.654(4) Å). Atom Eu(2), also non-acoordinate, is coordinated by five O atoms from three oxalate ligands and four O atoms from three carbonato ligands, but with no aqua ligands; the Eu2−O distances range from 2.433(5) to 2.654(5) Å. Each carbonato ligand bridges one Eu(1) and three Eu(2) atoms in a μ_4-η^2:η^2:η^2 fashion, resulting in a double-edge sawtooth-like lanthanide carbonate chain structure (Figure S1, Supporting Information). The oxalate ligands exhibit two different coordination modes, one being doubly chelating to form two five-membered rings, while the other being also doubly chelating but with one of its four O atoms (O5 in Figure 1) bridging an additional Eu1 atom. These chelating and bridging interactions lead to the formation of a 2D arrays of six-membered rings in the (100) plane (Figure S2, Supporting Information).

The lanthanide carbonate chains are connected by oxalate groups into 2D layers, and further into the overall 3D framework structure (Figure 2a). Along the crystallographic *a*-axis exist highly ordered hexagonal channels (diameter of about 6.8 Å) that are filled with guest water molecules (Figure S3, Supporting Information). Decorating the interior of the channels are aqua ligands (O3 and O12), two on each Eu(1) atom; they connect adjacent ox groups to form 1D hydrogen-bonding arrays (Figure 2b and Table S1, Supporting Information) that involve four sites of the hexagonal opening. The multiple and highly ordered hydrogen-bonding arrays suggest high proton conductivity, which was subsequently observed.

Conductivity Measurements Using Pellets of 1. The proton conduction behavior of **1** was studied by alternating current (AC) impedance measurements. At 25 °C and without

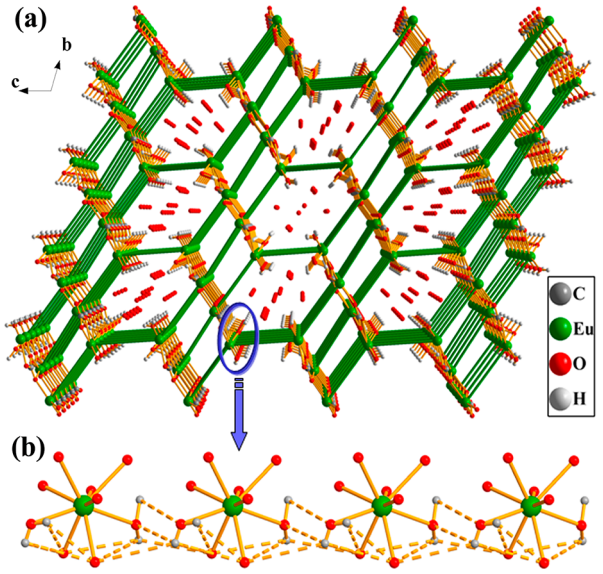

Figure 2. (a) The crystal structure for **1** showing the 1D channels along the *a*-axis filled with the free waters; the ox groups are simplified as the green bonds. (b) View showing the 1D hydrogen-bonded array of aqua ligands and adjacent oxalate groups in the direction of the *a*-axis.

any additional humidity, the as-synthesized microcrystalline sample was measured to have a conductivity of 9.21×10^{-6} S cm^{-1}. At 40% and 90% RH (Figure S8, Supporting Information), the corresponding values are 9.34×10^{-6} and 1.12×10^{-5} S cm^{-1}, respectively, with the former being essentially the same as and the latter representing only a modest increase over the humidity-independent values. Thus, RH does not appear to be a significant factor in determining the conductivity of **1**.

Subsequent AC impedance measurements were thus carried out free of any additional humidity over the temperature range of 25−200 °C (Figures S9−S12, Supporting Information). Typical impedance plots displaying a partial semicircle at high frequencies and a tail at lower frequencies were obtained. The impedance is largely originated from the bulk and grain-boundary resistance of the microcrystalline in addition to contributions from the electrode. The conductivity increased with temperature, quickly to 8.08×10^{-4} S cm^{-1} at about 100 °C, reaching a maximum of 2.08×10^{-3} S cm^{-1} at 150 °C before dropping precipitously with further increase of temperature (Figure 3). We believe that this latter value of conductivity, comparable to that of an acid-impregnated MOF, is the largest reported for any hydrated MOF materials whose proton conduction is solely mediated by water molecules, lattice or coordinated.[10]

Cooling a sample led to a decrease in its conductivity, and a value of 2.44×10^{-6} S cm^{-1} in the absence of any additional humidity was obtained at 25 °C (Figure 4). The small yet notable difference of conductivity at the same temperature between the as-prepared **1** and the dehydrated and then cooled sample may be rationalized by the loss of the crystallization water molecules in the latter. Even so, the conductivity at a particular temperature in both the heating and cooling processes between 25 and 150 °C are close to each other, in particular in the higher-temperature region. The conduction performance was stabilized after five cooling/heating cycles, as indicated by the superimposed traces of conductivity obtained

dx.doi.org/10.1021/ja5069855 | J. Am. Chem. Soc. 2014, 136, 12444−12449

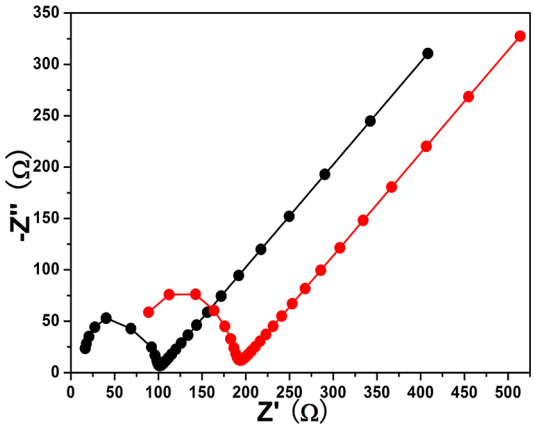

Figure 3. Impedance plots of **1** (black) and the deuterated **1** (red) at 150 °C and without additional humidity.

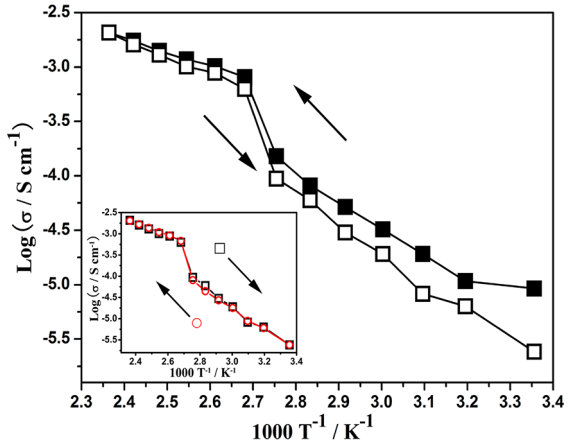

Figure 4. Arrhenius plots of conductivities of **1** from 25 to 150 °C and without additional humidity; heating cycle (■) and cooling cycle (□). (Inset) The proton conductivity of **1** during the cooling and reheating from 25 to 150 °C and without additional humidity; cooling cycle (□) and reheating cycle (○).

upon heating and cooling of the sample (inset, Figure 4); stable conduction is essential for possible practical applications of such materials in fuel cells. The powder X-ray diffraction (PXRD) pattern of the sample retrieved after five cooling/heating cycles is minimally altered when compared with that of the as-prepared sample of **1** (Figure S7, Supporting Information), thus indicating the stability of the present proton-conducting MOF and corroborating with the robust Arrhenius plots of conductivities (Figure 4).

Mechanistic Studies. The unusually high conductivity of **1** observed at temperatures above the boiling point of water up to 150 °C prompted us to carry out a number of studies with the attempt to gain mechanistic insights into the observed conduction in this unique Ln-MOF.

Our very first piece of effort was to establish the nature of the charge carrier for the observed conduction. Specifically, we carried our comparative conductivity measurements using as-prepared **1** and a deuterated sample under otherwise identical conditions. Similar conductivity−temperature relationship was revealed (Table S2, Supporting Information) with the deuterated sample producing a lower conductivity of 1.07×10^{-3} S cm^{-1} at 150 °C, consistent with proton being the charge carrier in the observed conduction process.[16a]

We then probed the temperature effect on the conductivity. In this context, three observations, all mentioned above, are relevant. First, with respect to an as-prepared sample, a slight decrease in conductivity of a sample cooled to 25 °C after its water molecules of crystallization were thermally removed suggested that these water molecules did contribute to the overall proton conduction. Second, from 25 up to 150 °C but prior to the loss of the crystallization water molecules, the increase of conductivity with temperature enhancement can be attributable to thermal activation of these water molecules and the aqua ligands. The rapid increase of conductivity commencing in the proximity of 100 °C is counterintuitive, as thermogravimetric analysis (Figure S4, Supporting Information) indicates the loss of crystallization water, and without any additional influences, this thermal loss of water is expected to cause a decrease rather than the observed increase in conductivity. A corollary is thus inferred that the remaining aqua ligands, and more exactly, the hydrogen-bonded arrays featuring the aqua and the oxalate ligands are probably responsible for mediating the transport of protons, and that conductivity increase associated with the thermal facilitation of proton transport within the hydrogen-bonded arrays prevails over the reduction due to the loss of crystallization water. Third, although the conductivity of **1** at 150 °C remained essentially constant for the experimental duration of 12 h (Figure S11, Supporting Information), it dropped with further increase in temperature, and precipitously to 3.26×10^{-7} S cm^{-1} at 160 °C (Figure S12, Supporting Information). This observation is consistent with the above argument as further increase of temperature thermally removed the aqua ligands, resulting in the disintegration of the hydrogen-bonded arrays and the putative pathway for proton conduction. However, as indicated by the minimally altered PXRD patterns (Figure S5, Supporting Information), the overall framework structure was able to sustain as high a temperature as 350 °C. The robustness of this potentially useful proton-conducting MOF was further revealed by the restoration of the original structure of **1** and the reproduction of its conduction behavior by rehydrating a sample that has been thermally activated at 250 °C (Figure S13, Supporting Information). Together, these results firmly establish that the hydrogen-bonded arrays are primarily responsible for the transport of protons and the observed charge conduction.

Since the hydrogen-bonded arrays extend along the crystallographic *a*-axis, we carried out conductivity measurements using a single crystal of **1** in order to directly demonstrate the conduction in this particular direction and to establish the anisotropic conduction of protons. The indexing of the surface of a large single crystal of **1** (0.71 cm × 0.14 cm × 0.11 cm, Figure 5a) was achieved by X-ray diffraction patterning. Specifically, with its showing of a (100) peak, the side surface of **1** as shown in Figure 5b was determined to be parallel to the *bc* plane, while its upper surface (Figure 5c) with the production of the (001) and (002) peaks was identified to be aligned with the *ab* plane. Its AC impedances were measured from 25 to 150 °C using the same procedure as previously applied toward the bulk microcrystalline sample (Table S2, Supporting Information). At 150 °C, the conductivity between two side-surfaces (*bc* plane) was 2.14×10^{-3} S cm^{-1} (Figure 5e), slightly above but essentially the same as the value (2.08×10^{-3} S cm^{-1}) obtained using a microcrystalline sample. However, the conductivity between the two upper surfaces (*ab* plane) was 4.86×10^{-7} S cm^{-1}, almost 4 orders of

dx.doi.org/10.1021/ja5069855 | J. Am. Chem. Soc. 2014, 136, 12444−12449

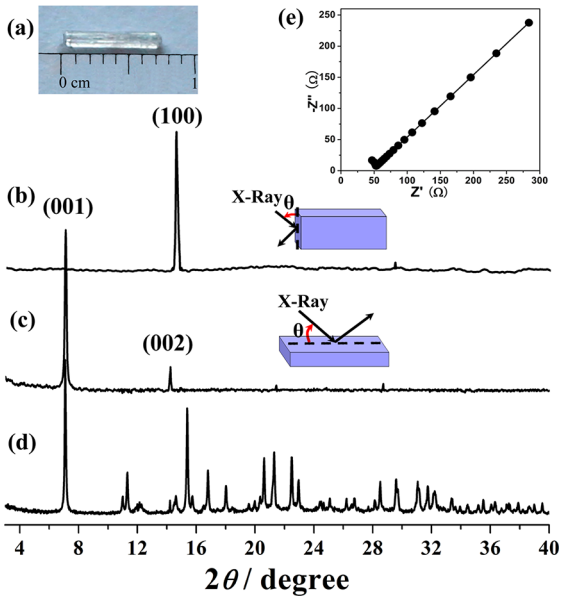

Figure 5. (a) The photo for the large single crystal of **1**. XRD patterns of the large single crystal of **1** scanned from 3 to 40° relative to the side plane (b) and the upper plane (c). (d) PXRD pattern of the as-synthesized **1**. (e) Impedance plot for the *bc* plan of **1** at 150 °C and without additional humidity.

magnitude smaller than that of the microcrystalline sample. The distinct conduction behaviors between these two crystal surfaces can be easily understood as the access to the conducting pathway, directional hydrogen-bonding in nature, is readily achieved in the *a*-axis (connecting the two side *bc* planes) but not along the *c*-axis (orthogonal to the hydrogen-bonded proton-transporting pathway). The preferred *a*-axis for proton conduction is not manipulated or even limited by water molecules of crystallization; rather it is determined by the ordered arrays of hydrogen bonding interactions. As such, even with the complete loss of crystallization water molecules at 150 °C, the conduction pathway was maintained with no showing of decrease in proton conductivity. Lending further support to this anisotropic proton conduction by way of hydrogen-bonded arrays was the drastically reduced conductivity to 7.94×10^{-8} S cm^{-1} along the *a*-axis when the temperature reached 160 °C at which the aqua ligands were also thermally removed, thus disrupting the conducting pathway for proton transport.

The activation energies, calculated by fitting the conductivity between the *bc* planes or along the *a*-axis to the Arrhenius equation, are 0.47 eV (25−90 °C) and 0.26 eV (100−150 °C) (Figure S14, Supporting Information), both being negligibly smaller than the corresponding values (0.49 and 0.28 eV, respectively) obtained with a microcrystalline sample. These results, on the one hand, reveal the profound temperature effect on proton conduction; they unambiguously establish that the 1D hydrogen-bonded array along the *a*-direction is the preferred pathway for proton-conduction. The much enhanced conductivity and the corresponding much lowered activation energy in the higher temperature range (100−150 °C) may be rationalized as such: When the temperature increases, rotation of the aqua ligands and the vibration of their O−H bonds facilitate the hopping of protons from the aqua ligands to adjacent oxalate groups within the hydrogen-bonded arrays, as reflected by the increased conductivity.

The above results point to the operation of the Grotthuss mechanism for proton conduction, corroborated also by the corresponding activation energy of 0.28 eV between 100 and 150 °C, calculated by fitting the proton conductivity data to the Arrhenius equation (Figure 4); an activation energy in the range of 0.1−0.4 eV is generally considered to be associated with the Grotthuss mechanism, whereas the vehicle mechanism, the other significant model for the interpretation of fast proton conduction, is generally more energetically demanding with activation energies in the range of 0.5−0.9 eV.[11i,18] Between 25 and 90 °C, the vehicle mechanism may be partially operative as suggested by the activation energy of 0.49 eV in this lower-temperature region. An abrupt increase in conductivity occurred in the proximity of 100 °C, attributable to the transition from a mixed Grotthuss and vehicle transport mechanism to predominantly if not exclusively the Grotthuss mechanism.

To understand in more detail the role of the aqua ligands, temperature-dependent photoluminescence properties of **1** were studied. The temperature dependence of the emission spectra from 25 to 150 °C is illustrated in Figure 6, and the

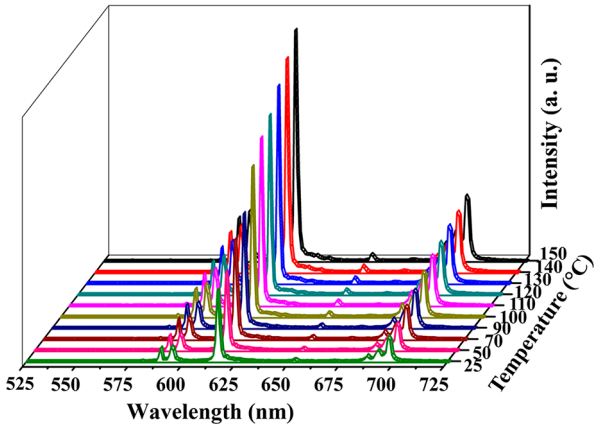

Figure 6. Emission spectra of **1** recorded between 25 and 150 °C (excited at 365 nm).

corresponding integrated intensities (Figure S15, Supporting Information) of the $^5D_0 \rightarrow {}^7F_2$ transition (616 nm) reveal the steady intensification of the characteristic red emission of Eu(III) with increasing temperature.

The lifetime of the $^5D_0$ excited state was also found to increase as temperature was enhanced (Figures S16−S21, Supporting Information). As vibronic coupling with O−H bonds is known to effectively quench the $^5D_0$ excited state and the extent of the quenching is directly related to the number of aqua ligands, the lifetime (τ in ms) of the excited state can be used to estimate the degree of hydration of Eu(III) by using the equation $n_{H2O} = 1.05\tau^{-1} - 0.70$, where n_{H2O} is the hydration number.[19,20] The temperature-dependent results at representative temperatures in the 25−150 °C range are collected in Table 1.

The single lifetime obtained reflects the effective coupling between the two distinct Eu(III) sites, due primarily to the extensive hydrogen bonding interactions and the intimate association reinforced by the bridging of both the carbonato and oxalate ligands. Similar observation of a shared lifetime for two different emissive lanthanide centers has previously been reported.[21] We note that the n_{H2O} at temperatures above 100 °C is smaller than 1. However, even $n_{H2O} = 0.76$ does not mean

dx.doi.org/10.1021/ja5069855 | J. Am. Chem. Soc. 2014, 136, 12444−12449

Table 1. Lifetime τ and n_{H2O} of 1 at Different Temperature

temperature (T/°C)	lifetime (τ/ms)	n_{H2O}
25	0.49	1.41
50	0.54	1.24
80	0.59	1.06
100	0.64	0.94
120	0.69	0.83
150	0.72	0.76

the removal of the aqua ligands as the thermal analysis of **1** detailed above suggested otherwise. Rather, it is a reflection of the elongation and weakening of the Eu−OH_2 coordinative bonds. Without breaking the ordered hydrogen-bonding array, a corollary is that the aqua ligands become more intimately associated with an adjacent oxalate group; this "mobilization" of the aqua ligands promotes transport of protons that is a key to the observed enhancement of proton conduction.

SUMMARY

We report the synthesis and structural characterization of a new Ln-MOF. Unlike previously reported MOFs whose proton conduction is achieved in the presence of additional humidity and typically at ambient temperature, the title microcrystalline material possesses humidity-independent high proton conductivity that maximizes well above the normal boiling point of water at 150 °C. Detailed structural analysis revealed within the MOF channels ordered 1D hydrogen-bonded arrays whose integrity was maintained up to 150 °C, but thermogravimetric studies indicate that the overall framework structure is sustained at a temperature as high as 350 °C. Comparative conduction measurements using both regular and deuterated samples point to proton as the charge carrier for the observed conduction. Variable-temperature anisotropic conduction measurements made on a single crystal of the MOF established that the observed proton conduction was achieved by way of the hydrogen-bonded arrays along its crystallographic *a*-axis. Results of variable-temperature photoluminescence studies suggest dynamic hydrogen-bonding interactions between the aqua and adjacent oxalate ligands, which provides a convincing scenario of proton transport by the Grotthuss mechanism and, most importantly, a rationalization for the observed enhancement of conductivity with increasing temperature. It appears that a combination of the thermal stability of the aqua ligands, activation via metal coordination of the water molecules for proton transport, and an appropriately structured pathway of hydrogen bonding for proton conduction is critical for the observed high proton conductivity. The humidity-independent high proton conduction, the wide working temperature range, and the stable performance sustaining multiple cooling/heating cycles make this and similar Ln-MOF materials potentially useful for fuel cell applications.

EXPERIMENTAL SECTION

Materials and Instruments. All reagents were commercially available and used as received. Microanalysis of C and H was performed on a PerkinElmer 2400 CHN elemental analyzer, while that of Eu was obtained using a PLASMA-SPEC(I) ICP atomic emission spectrometer. Thermogravimetric (TG) analyses were carried out by using a PerkinElmer TGA7 instrument, with a heating rate of 10 °C/min and under a nitrogen atmosphere. Powder X-ray diffraction (XRD) measurements were performed with a Rigaku D/MAX-3 instrument with Cu Kα radiation in the 2θ range of 3−60° at different temperatures.

Syntheses of $[Eu_2(CO_3)(ox)_2(H_2O)_2]\cdot 4H_2O$ (1). $Eu_2(CO_3)_3$ (96.8 mg, 0.2 mmol) and $H_2(ox)\cdot 2H_2O$ (25.2 mg, 0.2 mmol) were dissolved in 10 mL of deionized water. The mixture was stirred for 1 h at room temperature and then transferred to a 15 mL Teflon-lined stainless steel container. The reaction vessel was sealed and heated under autogenous pressure, first at 140 °C for 4 days and then at 100 °C for 10 h before being naturally cooled to room temperature. Colorless block-shaped crystals of **1** were collected by filtration, washed with deionized water, and dried (68% yield based on Eu). Anal. Calcd for $C_5H_{12}Eu_2O_{17}$ (%): C, 9.27; H, 1.87; Eu, 46.90. Found: C, 9.02; H, 1.95; Eu, 46.58. The elemental analysis for the sample **1** heated to 150 °C for 12 h (%, Calcd): C, 10.22 (10.43); H, 0.74 (0.70); Eu, 52.81 (52.76). The deuterated **1** was synthesized with the use of corresponding deuterated reagents using otherwise identical procedures. Anhydrous samples were obtained by heating the as-prepared **1** at 250 °C under dynamic vacuum for 24 h. Exposing the dehydrated sample in an environment of 90% relative humidity for 12 h reproduced pristine **1**.

Proton Conductivity Measurements. With a press and a die measuring 9.6 mm in diameter and 2.0 mm (±0.08%) in thickness, samples of **1** were pressed into disk-shaped pellets. Using a frequency response analyzer/potentiostat (Princeton Applied Research PAR-STAT 2273, EG&GPARC, Princeton, NJ) over a frequency range from 0.1 to 1 MHz, the impedances were measured with a quasi-four probe electrochemical cell using Ag-pressed electrodes under an applied ac voltage of 30 mV. Samples were equilibrated for at least 5 h prior to measurements that were taken in the temperature range of 25−200 °C and without additional humidity conditions. Samples were equilibrated for at least 5 h. ZSimpWin software was used to extrapolate impedance data results by means of an equivalent circuit simulation to complete the Nyquist plot and obtain the resistance values.

Photoluminescence Measurement. Photoluminescence spectra were obtained using a FLSP 920 Edinburgh instrument (Eng) with 450 W xenon lamp monochromatized by double grating. The luminescence decay curves measurements were carried out using Edinburgh Instruments FLSP 920 based on time correlated photon counting technique. The temperature of sample was equilibrated for at least 5 h.

ASSOCIATED CONTENT

Supporting Information

X-ray crystallographic data for **1**. X-ray crystallographic data and structural refinement, packing diagram, TG curve, powder XRD patterns, impedance plots, and decay curves. This material is available free of charge via the Internet at http://pubs.acs.org.

AUTHOR INFORMATION

Corresponding Authors

liusx@nenu.edu.cn.
zhiping@email.arizona.edu.

Notes

The authors declare no competing financial interest.

ACKNOWLEDGMENTS

This work was supported by the National Natural Science Foundation of China (Grants 21171032, 21371029 and 21231002), the Key Technologies R&D Program of Jilin Province of China (Grant 20130206079SF), and the Open Research Fund of the State Key Laboratory of Inorganic Synthesis and Preparative Chemistry (Jilin University, Grant 2015−01), and in part by US National Science Foundation (Grant CHE-1152609).

REFERENCES

(1) Kreuer, K.-D.; Paddison, S. J.; Spohr, E.; Schuster, M. *Chem. Rev.* **2004**, *104*, 4637−4678.

(2) (a) Kreuer, K.-D. *Chem. Mater.* **1996**, *8*, 610−641. (b) Laberty-Robert, C.; Valle, K.; Pereira, F.; Sanchez, C. *Chem. Soc. Rev.* **2011**, *40*, 961−1005. (c) Tolle, P.; Kohler, C.; Marschall, R.; Sharifi, M.; Wark, M.; Frauenheim, T. *Chem. Soc. Rev.* **2012**, *41*, 5143−5159.

(3) (a) Li, S.-L.; Xu, Q. *Energy Environ. Sci.* **2013**, *6*, 1656−1683. (b) Ohkoshi, S.-i.; Nakagawa, K.; Tomono, K.; Imoto, K.; Tsunobuchi, Y.; Tokoro, H. *J. Am. Chem. Soc.* **2010**, *132*, 6620−6621.

(4) (a) Mauritz, K. A.; Moore, R. B. *Chem. Rev.* **2004**, *104*, 4535−4586. (b) Yoon, M.; Suh, K.; Kim, H.; Kim, Y.; Selvapalam, N.; Kim, K. *Angew. Chem., Int. Ed.* **2011**, *50*, 7870−7873. (c) Gu, W.; Zhou, B.; Geyer, T.; Hutter, M.; Fang, H.; Helms, V. *Angew. Chem., Int. Ed.* **2011**, *50*, 768−771. (d) Zhou, Y.; Yang, J.; Su, H.; Zeng, J.; Jiang, S. P.; Goddard, W. A. *J. Am. Chem. Soc.* **2014**, *136*, 4954−4964.

(5) (a) Li, J.-R.; Kuppler, R. J.; Zhou, H.-C. *Chem. Soc. Rev.* **2009**, *38*, 1477−1504. (b) Suh, M. P.; Park, H. J.; Prasad, T. K.; Lim, D.-W. *Chem. Rev.* **2011**, *112*, 782−835. (c) Li, J.-R.; Sculley, J.; Zhou, H.-C. *Chem. Rev.* **2011**, *112*, 869−932.

(6) (a) Yoon, M.; Srirambalaji, R.; Kim, K. *Chem. Rev.* **2011**, *112*, 1196−1231. (b) Lee, J.; Farha, O. K.; Roberts, J.; Scheidt, K. A.; Nguyen, S. T.; Hupp, J. T. *Chem. Soc. Rev.* **2009**, *38*, 1450−1459. (c) Gu, Z.-Y.; Park, J.; Raiff, A.; Wei, Z.; Zhou, H.-C. *ChemCatChem* **2014**, *6*, 67−75.

(7) (a) Kreno, L. E.; Leong, K.; Farha, O. K.; Allendorf, M.; Van Duyne, R. P.; Hupp, J. T. *Chem. Rev.* **2011**, *112*, 1105−1125. (b) Rocha, J.; Carlos, L. D.; Paz, F. A.; Ananias, D. *Chem. Soc. Rev.* **2011**, *40*, 926−940. (c) Binnemans, K. *Chem. Rev.* **2009**, *109*, 4283−4374. (d) Liu, D.; Lu, K.; Poon, C.; Lin, W. *Inorg. Chem.* **2014**, *53*, 1916−1924. (e) He, J.; Zha, M.; Cui, J.; Zeller, M.; Hunter, A. D.; Yiu, S.-M.; Lee, S.-T.; Xu, Z. *J. Am. Chem. Soc.* **2013**, *135*, 7807−7810.

(8) (a) Yoon, M.; Suh, K.; Natarajan, S.; Kim, K. *Angew. Chem., Int. Ed.* **2013**, *52*, 2688−2700. (b) Yamada, T.; Otsubo, K.; Makiura, R.; Kitagawa, H. *Chem. Soc. Rev.* **2013**, *42*, 6655−6669.

(9) (a) Shimizu, G. K.; Taylor, J. M.; Kim, S. *Science* **2013**, *34*, 354−355. (b) Horike, S.; Umeyama, D.; Kitagawa, S. *Acc. Chem. Res.* **2013**, *46*, 2376−2384.

(10) Ramaswamy, P.; Wong, N. E.; Shimizu, G. K. H. *Chem. Soc. Rev.* **2014**, *43*, 5913−5932.

(11) (a) Nagarkar, S. S.; Unni, S. M.; Sharma, A.; Kurungot, S.; Ghosh, S. K. *Angew. Chem., Int. Ed.* **2014**, *53*, 2638−2642. (b) Xu, G.; Otsubo, K.; Yamada, T.; Sakaida, S.; Kitagawa, H. *J. Am. Chem. Soc.* **2013**, *135*, 7438−7441. (c) Taylor, J. M.; Dawson, K. W.; Shimizu, G. K. *J. Am. Chem. Soc.* **2013**, *135*, 1193−1196. (d) Kitagawa, H.; Nagao, Y.; Fujishima, M.; Ikeda, R.; Kanda, S. *Inorg. Chem. Commun.* **2003**, *6*, 346−348. (e) Okawa, H.; Sadakiyo, M.; Yamada, T.; Maesato, M.; Ohba, M.; Kitagawa, H. *J. Am. Chem. Soc.* **2013**, *135*, 2256−2262. (f) Horike, S.; Kamitsubo, Y.; Inukai, M.; Fukushima, T.; Umeyama, D.; Itakura, T.; Kitagawa, S. *J. Am. Chem. Soc.* **2013**, *135*, 4612−4615. (g) Sen, S.; Nair, N. N.; Yamada, T.; Kitagawa, H.; Bharadwaj, P. K. *J. Am. Chem. Soc.* **2012**, *134*, 19432−19437. (h) Sadakiyo, M.; Okawa, H.; Shigematsu, A.; Ohba, M.; Yamada, T.; Kitagawa, H. *J. Am. Chem. Soc.* **2012**, *134*, 5472−5475. (i) Shigematsu, A.; Yamada, T.; Kitagawa, H. *J. Am. Chem. Soc.* **2011**, *133*, 2034−2036. (j) Jeong, N. C.; Samanta, B.; Lee, C. Y.; Farha, O. K.; Hupp, J. T. *J. Am. Chem. Soc.* **2012**, *134*, 51−54.

(12) (a) Liang, X.; Zhang, F.; Feng, W.; Zou, X.; Zhao, C.; Na, H.; Liu, C.; Sun, F.; Zhu, G. *Chem. Sci.* **2013**, *4*, 983−992. (b) Colodrero, R. M. P.; Papathanasiou, K. E.; Stavgianoudaki, N.; Olivera-Pastor, P.; Losilla, E. R.; Aranda, M. A. G.; León-Reina, L.; Sanz, J.; Sobrados, I.; Choquesillo-Lazarte, D.; García-Ruiz, J. M.; Atienzar, P.; Rey, F.; Demadis, K. D.; Cabeza, A. *Chem. Mater.* **2012**, *24*, 3780−3792. (c) Sahoo, S. C.; Kundu, T.; Banerjee, R. *J. Am. Chem. Soc.* **2011**, *133*, 17950−17958. (d) Zhu, M.; Hao, Z. M.; Song, X. Z.; Meng, X.; Zhao, S. N.; Song, S. Y.; Zhang, H. J. *Chem. Commun.* **2014**, *50*, 1912−1914. (e) Pardo, E.; Train, C.; Gontard, G.; Boubekeur, K.; Fabelo, O.; Liu, H.; Dkhil, B.; Lloret, F.; Nakagawa, K.; Tokoro, H.; Ohkoshi, S.-i.; Verdaguer, M. *J. Am. Chem. Soc.* **2011**, *133*, 15328−15331. (f) Kim, S.; Dawson, K. W.; Gelfand, B. S.; Taylor, J. M.; Shimizu, G. K. *J. Am. Chem. Soc.* **2013**, *135*, 963−966. (g) Costantino, F.; Donnadio, A.; Casciola, M. *Inorg. Chem.* **2012**, *51*, 6992−7000.

(13) (a) Yamada, T.; Sadakiyo, M.; Kitagawa, H. *J. Am. Chem. Soc.* **2009**, *131*, 3144−3145. (b) Ōkawa, H.; Shigematsu, A.; Sadakiyo, M.; Miyagawa, T.; Yoneda, K.; Ohba, M.; Kitagawa, H. *J. Am. Chem. Soc.* **2009**, *131*, 13516−13522. (c) Sadakiyo, M.; Yamada, T.; Kitagawa, H. *J. Am. Chem. Soc.* **2009**, *131*, 9906−9907. (d) Panda, T.; Kundu, T.; Banerjee, R. *Chem. Commun.* **2013**, *49*, 6197−6199. (e) Panda, T.; Kundu, T.; Banerjee, R. *Chem. Commun.* **2012**, *48*, 5464−5466. (f) Wei, M.; Wang, X.; Duan, X. *Chem.—Eur. J.* **2013**, *19*, 1607−1616.

(14) (a) Taylor, J. M.; Mah, R. K.; Moudrakovski, I. L.; Ratcliffe, C. I.; Vaidhyanathan, R.; Shimizu, G. K. H. *J. Am. Chem. Soc.* **2010**, *132*, 14055−14057. (b) Morikawa, S.; Yamada, T.; Kitagawa, H. *Chem. Lett.* **2009**, *38*, 654−655. (c) Colodrero, R. M. P.; Olivera-Pastor, P.; Losilla, E. R.; Hernández-Alonso, D.; Aranda, M. A. G.; Leon-Reina, L.; Rius, J.; Demadis, K. D.; Moreau, B.; Villemin, D.; Palomino, M.; Rey, F.; Cabeza, A. *Inorg. Chem.* **2012**, *51*, 7689−7698. (d) Meng, X.; Song, X.-Z.; Song, S.-Y.; Yang, G.-C.; Zhu, M.; Hao, Z.-M.; Zhao, S.-N.; Zhang, H.-J. *Chem. Commun.* **2013**, *49*, 8483−8485. (e) Mallick, A.; Kundu, T.; Banerjee, R. *Chem. Commun.* **2012**, *48*, 8829−8831.

(15) (a) Colodrero, R. M. P.; Angeli, G. K.; Bazaga-Garcia, M.; Olivera-Pastor, P.; Villemin, D.; Losilla, E. R.; Martos, E. Q.; Hix, G. B.; Aranda, M. A. G.; Demadis, K. D.; Cabeza, A. *Inorg. Chem.* **2013**, *52*, 8770−8783. (b) Liang, X.; Zhang, F.; Zhao, H.; Ye, W.; Long, L.; Zhu, G. *Chem. Commun.* **2014**, *50*, 6513−6516. (c) Bazaga-Garcia, M.; Colodrero, R. M.; Papadaki, M.; Garczarek, P.; Zon, J.; Olivera-Pastor, P.; Losilla, E. R.; Leon-Reina, L.; Aranda, M. A.; Choquesillo-Lazarte, D.; Demadis, K. D.; Cabeza, A. *J. Am. Chem. Soc.* **2014**, *13*, 5731−5739.

(16) (a) Hurd, J. A.; Vaidhyanathan, R.; Thangadurai, V.; Ratcliffe, C. I.; Moudrakovski, I. L.; Shimizu, G. K. H. *Na.t Chem.* **2009**, *1*, 705−710. (b) Umeyama, D.; Horike, S.; Inukai, M.; Itakura, T.; Kitagawa, S. *J. Am. Chem. Soc.* **2012**, *134*, 12780−12785. (c) Umeyama, D.; Horike, S.; Inukai, M.; Kitagawa, S. *J. Am. Chem. Soc.* **2013**, *135*, 11345−11350. (d) Ponomareva, V. G.; Kovalenko, K. A.; Chupakhin, A. P.; Dybtsev, D. N.; Shutova, E. S.; Fedin, V. P. *J. Am. Chem. Soc.* **2012**, *134*, 15640−15643. (e) Umeyama, D.; Horike, S.; Inukai, M.; Hijikata, Y.; Kitagawa, S. *Angew. Chem., Int. Ed.* **2011**, *50*, 11706−11709.

(17) (a) Bureekaew, S.; Horike, S.; Higuchi, M.; Mizuno, M.; Kawamura, T.; Tanaka, D.; Yanai, N.; Kitagawa, S. *Nat. Mater.* **2009**, *8*, 831−836. (b) Horike, S.; Umeyama, D.; Inukai, M.; Itakura, T.; Kitagawa, S. *J. Am. Chem. Soc.* **2012**, *134*, 7612−7615. (c) Inukai, M.; Horike, S.; Umeyama, D.; Hijikata, Y.; Kitagawa, S. *Dalton Trans.* **2012**, *41*, 13261−13263.

(18) Ludueña, G. A.; Kühne, T. D.; Sebastiani, D. *Chem. Mater.* **2011**, *23*, 1424−1429.

(19) Chen, B.; Wang, L.; Zapata, F.; Qian, G.; Lobkovsky, E. B. *J. Am. Chem. Soc.* **2008**, *130*, 6718−6719.

(20) (a) Harbuzaru, B. V.; Corma, A.; Rey, F.; Atienzar, P.; Jordá, J. L.; García, H.; Ananias, D.; Carlos, L. D.; Rocha, J. *Angew. Chem., Int. Ed.* **2008**, *47*, 1080−1083. (b) Harbuzaru, B. V.; Corma, A.; Rey, F.; Jordá, J. L.; Ananias, D.; Carlos, L. D.; Rocha, J. *Angew. Chem., Int. Ed.* **2009**, *48*, 6476−6479. (c) Horrocks, W. D.; Sudnick, D. R. *J. Am. Chem. Soc.* **1979**, *101*, 334−340.

(21) (a) Dickins, R. S.; Parker, D.; de Sousa, A. S.; Williams, J. A. G. *Chem. Commun.* **1996**, 697−698. (b) Kim; Suh, M.; Jung, D.-Y. *Inorg. Chem.* **2004**, *43*, 245−250.